energies

MDPI

Article

Integrated Motor Drive: Mass and Volume Optimization of the Motor with an Integrated Filter Inductor †

Muhammad Raza Khowja [1,*], Gaurang Vakil [1], Chris Gerada [1,2], Chintan Patel [1], Shafiq Odhano [3] and Patrick Wheeler [1]

[1] Power Electronics, Machines and Control (PEMC) Research Group, University of Nottingham, Nottingham NG7 2RD, UK; Gaurang.Vakil@nottingham.ac.uk (G.V.); Chris.Gerada@nottingham.ac.uk (C.G.); crpatel19@gmail.com (C.P.); Pat.Wheeler@nottingham.ac.uk (P.W.)
[2] Department of Electrical and Electronic Engineering, University of Nottingham Ningbo China, Ningbo 315100, China
[3] School of Engineering, Newcastle University, Newcastle Upon Tyne NE1 7RU, UK; shafiq.odhano@newcastle.ac.uk
* Correspondence: Raza.Khowja@nottingham.ac.uk
† This paper is an extended version of our paper published in IECON 2016—42nd Annual Conference of the IEEE Industrial Electronics Society, Florence, Italy, 24–27 October 2016; pp. 2827–2832, doi:10.1109/IECON.2016.7793027.

Abstract: The present trend of aerospace industries is being shifted towards a "More Electric Aircraft" system which needs to be high power dense. For this purpose, the integration technologies have gained massive interest, providing the benefits of reduced losses, weight, volume and cost. In this article, the integration concept of a passive filter inductor is presented for a permanent magnet synchronous motor. The integrated motor eliminates the need of an external inductor, thus, eliminates the added inductor losses, mass, volume and cost associated with it. The motor utilizes its's inherent inductance to use it as a filter inductor instead of implementing a discrete inductor that is commonly placed between inverter and the motor terminals. Optimization study is carried out, where the filter branch windings are tapped, in terms of improving mass and volume and performance parameters such as power losses and torque ripple. From the optimization study, the motor with minimum weight and volume is experimentally validated at the rated conditions, in order to prove the concept feasibility. Total system weight and volume of integrated and traditional motor drives are compared, which gives the minimum weight of 2.26 kg and 3.14 kg respectively, and the minimum volume of 0.54 L and 1.1 L respectively.

Keywords: passive components; inductor; capacitor; integrated motor; filter branch windings; motor branch windings and aerospace applications

Citation: Khowja, M.R.; Vakil, G.; Gerada, C.; Patel, C.; Odhano, S.; Wheeler, P. Integrated Motor Drive: Mass and Volume Optimization of the Motor with an Integrated Filter Inductor. *Energies* **2021**, *14*, 4564. https://doi.org/10.3390/en14154564

Academic Editor: Mauro Andriollo

Received: 11 June 2021
Accepted: 20 July 2021
Published: 28 July 2021

1. Introduction

The continuous development of aircraft transportation, the demand for performance optimization and the need of reducing both weight and volume have pushed the aerospace industries to shift toward "More Electric Aircraft". As a result of this trend, mechanically-driven pumps, actuators and compressors are being replaced by electrical machines that reduce mechanical linkages within the aircraft system. For aerospace applications, the main objective is to minimize the weight and volume, and maximize the efficiency and the reliability of such electrical machines [1,2]. An interesting fact is that each kg gain in onboard aircraft increases the price by approximately 1000 USD on each flight so 1 kg saved in an aircraft can result in a saving of approximately 1700 tons of fuel and 5400 tons of CO_2 per annum, for all civil air traffic [3].

Passive components such as capacitors, inductors and transformers, associated with the electric motor drive systems, are employed for several purposes such as (1) low order

harmonics mitigation at the grid-side (2) to smooth out voltage ripples on the DC bus (3) and to protect the stator winding's insulation against the over-voltages and high dv/dt and to minimize torque ripple and high frequency losses at the machine-side [4]. These passives occupy a substantial amount of volume which impose penalties of potential higher mass and power loss, contributing a significant portion of converter's weight and volume which is potentially larger than 50% [4–6]. Traditionally, passive elements are designed, sized and introduced after the motor drive system's components have been defined, thus, resulting in a discrete sub-system. To overcome these drawbacks, the integration of passives needs to be introduced from a physical and functional perspective which leads to a compact design, reduced losses, weight, space and cost reduction, and fewer construction tasks. Therefore, applications where high power or torque-density is required, the use of the integrated technologies provides the finest solution [7].

The integrated motor-drives system, commonly known as IMDs, have been a focus of research in aerospace industry in the recent past, due to its compactness. There are many possibilities in the motor drive system to integrate the passive components. The use of the integration concept, in motor drive system, allows physical and functional integration of different drive components into a single component, resulting in a compact overall system, reduced cost, mass, volume and manufacturing and prototyping tasks [7,8]. Recently, the integration of passives has been investigated for motor drive applications. In [9,10], a new approach to integrate RLC output filter inductor is by using the motor's inherent inductance which divides the main motor windings into filter branch and the motor branch windings. This eliminates the need of adopting a separate filter inductor outside the motor housing, resulting in reduction of power losses, mass and volume associated with the motor drive system. The concept is experimentally validated in [9] with an in-depth comparative analysis between integrated and traditional motor drive systems, in terms of power quality, power losses, weight and volume. The reduction in total losses, in the motor with integrated filter inductor (IFI), by 34.2% were reported at 2.1 kRPM and 3 Nm load, compared to the motor with traditional EE-core filter inductor (TFI), whereas inductor's mass and space in the motor with IFI is eliminated entirely. In [4,11], structural integration of passive filter inductors was introduced within the common machine's housing. The presented inductors (i.e., rotational and rotor-less inductors) were integrated in the axial direction alongside the motor whilst sharing a common cooling system. Thus, eliminating the need of an additional cooling to take the heat out generated in the windings of filter inductor, when they are designed for high current density values. The rotational inductor's rotor rotates at the synchronous speed of the stator to reduce the magnetic losses through the rotor back iron. On the other hand, the rotor-less inductor has a similar construction prototype but without having any rotor back iron which makes it appropriate for isolation transformers, DC-link smoothing inductors and AC grid side input filters. In comparison, the rotational inductor can only be used for high-speed motor drive systems, with the advantage of reducing a portion of the magnetic loss inside the rotor. In [12], a design of an integrated rotor-less inductor is presented which to be implanted for 45 kW motor-drive in aircraft applications. The impact of high current density, on inductor's mass and volume, has been investigated and compared against the conventional EE-core inductor. The total mass and volume of the integrated inductor are reduced by 55.4% and 52.7% respectively, whereas the mass and volume of the combined system (i.e., machine + integrated inductor) are significantly reduced by 25.5% and 29.1% respectively. The increase in the winding loss due to high inductor's current density is taken out by the existing cooling system of the machine i.e., the inductor's stator is flooded with the engine oil alongside the machine's stator.

In [13], the stator yoke is completely utilized as a magnetic part for one or more separate toroidal winding inductors. This allows the alternate magnetic flux in the complete loop through the yoke of the stator iron core. If the yoke of the motor is operating in the linear magnetic region, then, the presence of ring flux, in the yoke, due to toroidal winding, will not affect the main flux. The drawback of this approach is the reduction of slot area

for the main winding, due to the addition of toroidal winding, which increases either the copper losses of the main motor or weight of the copper if the slot area is increased. Authors of [14,15] presented a physical integration of two grid-side input passive filters i.e., LCL inside the high-speed PMSM. The inductors are placed on the outermost slots of the motor. The inductor wounded on the outermost slots is optimized in terms of volume, copper loss and iron loss which is then compared against the conventional EE-core inductors. The integrated inductor is magnetically isolated and does not interact with the main motor flux. This is done by adopting different pole numbers of filter windings to that of torque producing main motor windings.

Inductors integrated onto the power modules substrate are presented in [16,17] with an aim of integrating inductor on power module substrates along with the switching devices, to increase its power density and improve thermal management. The concept is to make a bonding copper U-shapes which is representative of single winding turn on the substrate that enhances thermal exchange between the inductor and the cooling system, leading to an increased current density and hence reduction in mass and volume. From the manufacturing viewpoint, the power devices and inductor are bonded on the same Aluminium Nitride (AlN) Direct Bonded Copper (DBC) substrate that results in a uniform thermal distribution as opposed to the conventional standard inductors where the only input and output terminals are electrically and hence thermally connected to the substrate.

The main contributions of the paper include,

- Optimizing the motor-drive with IFI, introduced in [9,10], in terms of torque ripple, total system power losses, mass and volume which is then compared against the conventional standard motor-drive system (i.e., motor with TFI).
- This is done by adjusting the percentage of the filter branch windings from 10% to 50% of the entire motor windings, under consideration. For this purpose, the finite element (FE) and MATLAB/Simulink packages are used to model both conventional and integrated motor-drive systems and evaluate their performances.
- Since the main requirement of the application is to minimize overall system mass and space, therefore, machine with minimum weight and volume outcome from this study is experimentally tested and validated.

In the following section, the modelling of the traditional motor drive system is presented followed by the modelling of the motor with IFI in Section 3. In Section 4, filter branch optimization is discussed, where the filter branch is optimized aiming to minimize the system weight and volume and reduce the torque ripple and power losses. The experimental validation of the motor with IFI is given in Section 5 followed by the conclusive remarks in Section 6.

2. Motor Drive Application

The target application is a helicopter electro-mechanical actuation system (HEMAS) that provides the fault tolerance of individual jamming of an actuator whilst replacing the hydraulic actuator of a modern fly-by-wire hydraulic primary flight control system.

Each actuator is driven by a fault-tolerant PM machine, as shown in Figure 1, fed through individual inverters. The system provides the required performance after a mechanical damage or failure of a component (i.e., freewheel or jam) or two failures of electrical/electronic components (i.e., power electronics converter or motor). To accommodate a mechanical failure of the output mechanism a disconnect device is required to decouple an actuator in case of a jam or freewheel [18,19].

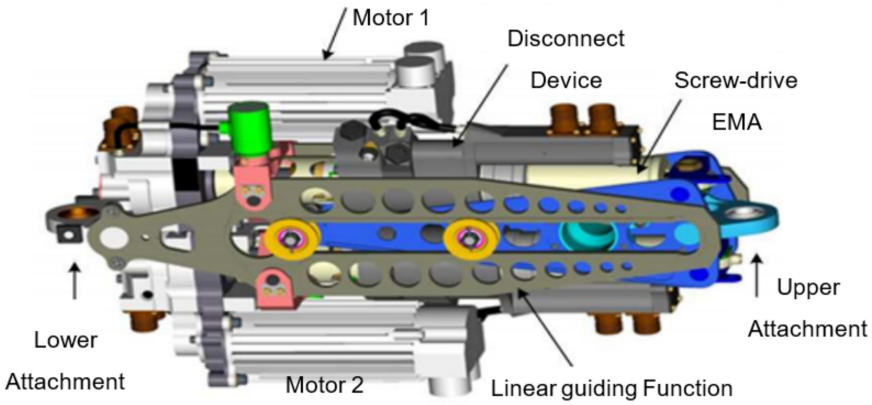

Figure 1. Helicopter electro-mechanical actuation system.

3. Traditional Motor Drive System

3.1. Motor Modelling

In traditional motor drive system, motor can be either modelled in dq frame or abc frame. In general, the motor is usually modelled and controlled in dq reference frame. Referring to the phasor of PMSM in Figure 2, the steady-state dq voltages in the synchronous reference frame for a three-phase machine (non-salient pole) are given as [20],

$$V_d = R_s I_d - L_q I_q \omega_e \tag{1}$$

$$V_q = R_s I_q + I_d L_d \omega_e + \lambda_m \omega_e \tag{2}$$

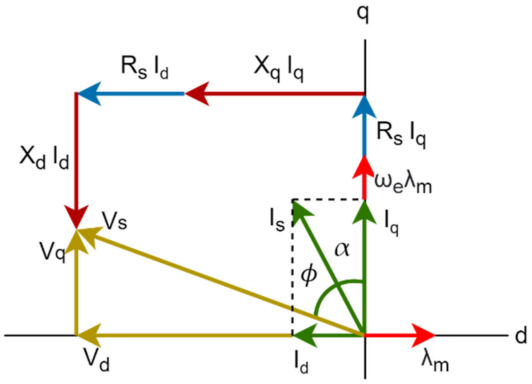

Figure 2. Phasor Diagram of Traditional PMSM.

The steady-state phase current and voltage can be obtained as

$$I_s = \sqrt{{I_q}^2 + {I_d}^2} \tag{3}$$

$$V_s = \sqrt{{V_q}^2 + {V_d}^2} \tag{4}$$

The electromagnetic torque (T_{em}) developed by the non-salient permanent magnet synchronous machine is,

$$T_{em} = K_t \lambda_m i_q \tag{5}$$

where, K_t is torque constant, λ_m is the PM flux (or no-load flux linkage) and i_q is the q-axis current.

3.2. Filter Modelling

The RLC output filter, as shown in Figure 3a, is the most, commonly, used filter which mitigates the converter switching harmonics injecting into the electrical machines. Thus, protecting the winding's insulation against the high voltages and minimizes the losses and torque ripple caused by the high frequencies [9]. The filter is designed by selecting the cut-off frequency of the filter which is given by (6),

$$f_{cut} = \frac{1}{2\pi\sqrt{L_F C_F}} \tag{6}$$

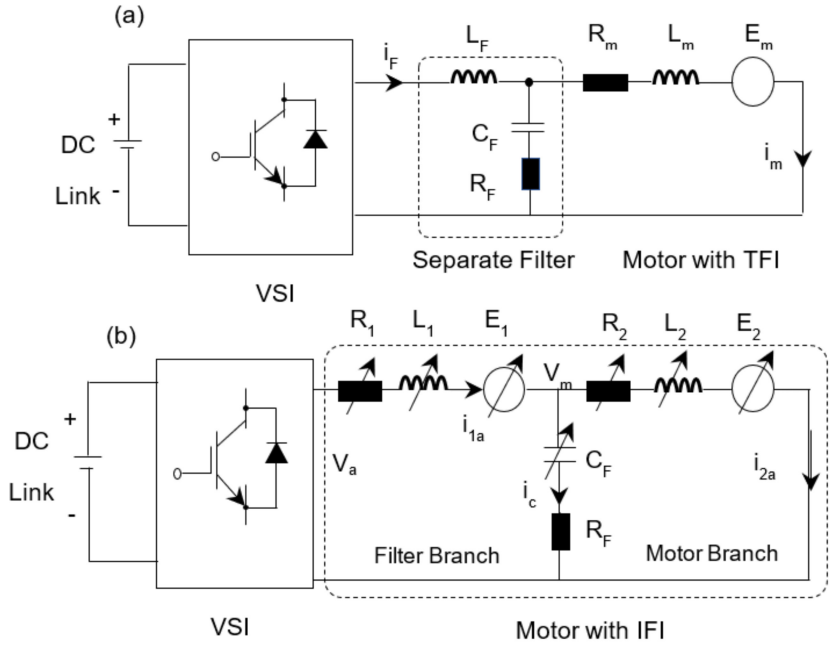

Figure 3. Motor Drive Systems (**a**) Motor with TFI (**b**) Motor with IFI.

In the literature, there are several guidelines for selecting the cut-off frequency for a filter circuit. In [21,22], it has been suggested to choose a cut-off frequency 10 times greater than the frequency of the motor current and less than 1/3rd of switching frequency of the power converter, which results in upper and lower bound as,

$$10 f_{out} < f_{cut} < \frac{1}{3} f_{sw} \tag{7}$$

The selection criteria of filter capacitance is used to avoid the interaction of control loop with the resonance between motor inductive reactance. Therefore,

$$C_F \leq \frac{1}{\omega_{max}{}^2 . L_m} \tag{8}$$

where L_m is the machine's inductance and ω_{max} is the maximum frequency that the current loop is able to reject. To damp the oscillation of the filter circuit, caused by the LC resonance, the damping resistance (R_F) is included in series with the filter capacitance(C_F), which reduces the undesirable oscillations caused by the resonance of L_F and C_F [22]. The value of the damping resistor can be determined by (9),

$$R_F = \frac{1}{3\omega_{cut} C_F} \tag{9}$$

4. Integrated Motor Drive System

4.1. Motor Modelling

For integrated motor drive system, motor is controlled in dq reference frame and modelled in *abc* reference frame due to the addition of filter capacitance and filter resistance. From Figure 3b, it can be seen that the motor with IFI is separated into two branches i.e., filter branch and the motor branch. The windings in the motor branch experience the sine-wave currents and voltages, whereas, high frequency currents will pass through the filter branch windings, which is tapped for the purpose optimization in terms of weight, volume, loss and torque ripple. The equations for filter branch currents and the motor branch currents (i.e., i_{1abc} and i_{2abc}), needed to model the motor with IFI, are determined using the single phase equivalent circuit as shown in Figure 3b. The mathematical model of the motor currents (i.e., three-phase filter branch and motor branch currents) can be obtained by applying mesh analysis on filter branch circuit (Figure 3), the derivation of which can be found in [9].

$$i_{1abc} = \frac{1}{sL_1}\left(V_{abc} + \omega_e \lambda_{m1} \sin\theta_e - R_1 i_{1abc} - R_F i_{1abc} + R_F i_{2abc} - \frac{1}{sC_F} i_{1abc} + \frac{1}{sC_F} i_{2abc}\right) \tag{10}$$

$$i_{2abc} = \frac{1}{sL_2}\left(0 + \omega_e \lambda_{m2} \sin\theta_e - R_2 i_{2abc} - R_F i_{2abc} + R_F i_{1abc} - \frac{1}{sC_F} i_{2abc} + \frac{1}{sC_F} i_{1abc}\right) \tag{11}$$

The torque components produced by the motor with IFI are (1) torque produced by filter branch windings, T_1 (2) torque produced by motor branch windings, T_2. Therefore, the output torque produced by the motor with IFI is,

$$T_{out} = T_1 + T_2 \tag{12}$$

$$T_{out} = K_t(\lambda_{m1} i_1 + \lambda_{m2} i_2 \cos\alpha) \tag{13}$$

where, λ_{m1} and λ_{m2} are the no-load flux linkages of filter and motor branch respectively, i_1 is the filter branch current which is equal to the q-axis current of filter branch, i_2 is motor branch current, $i_2 \cos\alpha$ is q-axis motor branch current, α, given by (14), is the phase-shift between the filter and motor branch currents due to the addition of filter capacitance and resistance, in the filter circuit. This phase-shift is very small since RC circuit is always designed to behave as a high impedance path at low frequencies and low impedance path beyond the cut-off frequencies, which will allow the switching ripple components to pass through it. The control of the motor (Figure 4 of [9]) with IFI is unchanged, the in-depth detail of which is reported in [9,10] where, the model of the motor with IFI is based on the "abc" reference frame. The "abc" currents are transformed into a dq reference frame in order to control the currents of their respective filter and motor branch windings.

$$\alpha = \cos^{-1}\left(\frac{i_1^2 + i_2^2 - i_c^2}{2\, i_1 i_2}\right) \tag{14}$$

4.2. Filter Modelling and Inductor Integration

The filter modelling or the estimation of filter parameters i.e., L_F, C_F and R_F follow the same guidelines as recommended in Section 3.2, for traditional motor drive system. The physical integration of inductor is illustrated in Figure 4, where a, 12 slots and 10 poles machine is used for the application helicopter actuation system [9,10]. The machine's stator is a single layer concentrated wound to achieve physical, thermal, and electrical separation between the phases. The rotor is constructed with "Halbach array" permanent magnets, mounted on the surface of the rotor, which is commonly used to increase the machine's power density.

The motor windings are separated into two branch windings i.e., filter branch windings and the motor branch windings. The phases A_2, B_2 C_2 belong to the motor branch, whereas the phases A_1, B_1 C_1 corresponds to the filter branch. The phases of motor branch

(A_2, B_2 C_2) and the filter branch (A_1, B_1 C_1) are wound in such an arrangement that the magnetic flux induced by both branch windings are cumulative. Initially, the motor has a total inductance of 1.3 mH which corresponds to 46 turns per coil. However, the portion of the filter branch windings can be varied in order to change filter branch inductance, thus, resulting in a higher portion of motor branch facing the filtered currents and voltages. At the same time, the reduction in filter branch inductance will increase the need of filter capacitance for the same attenuation level and the cut-off frequency. Considering the aforementioned approach, the filter branch is taped which uses a part of the main motor windings to provide an integrated inductance. In this case, the number of turns in the filter branch windings will reduce through the tapings, depending on the filter branch inductance, and the left-over motor turns will be added to the motor branch after connecting the filter capacitor and damping resistor.

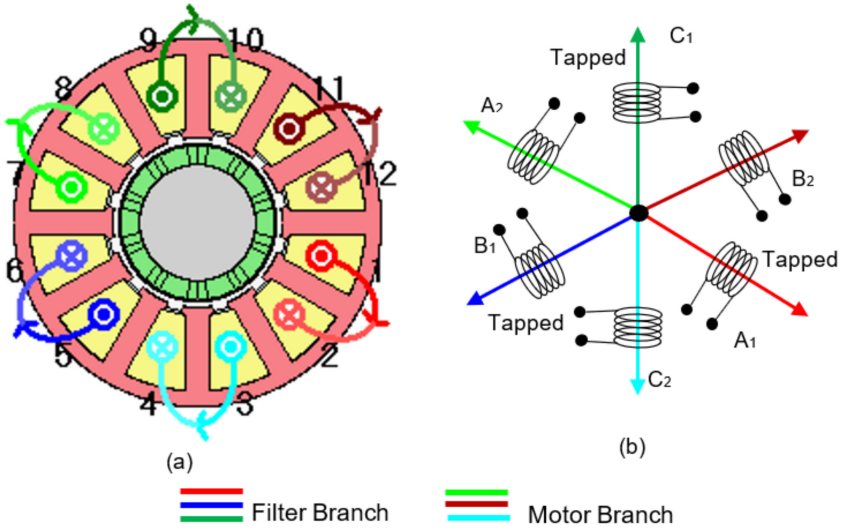

Figure 4. Motor with IFI (**a**) Radial cross-section (**b**) Motor Phasors.

5. Performance Optimization

The filter branch of the motor with IFI is optimized, in this section, focusing on improving the performance of the motor in terms of reducing total system losses, torque ripple and to evaluate the optimal inductance point where system weight and volume are minimum, which is the stringent requirement of the actuation system. The value of filter branch inductance is varied by modifying the coil turns in the filter branch, the details of which are illustrated in Table 1 and the details of the motor drive's parameters are shown in Table 2.

Table 1. Parameters of Traditional & Integrated Motor Drive.

$L_F = L_1$ (mH)	C_F (μF)	N_F (Filter Branch)	N_M (Filter Branch)	% Portion of the Filter Branch
0.28	22.5	10	82	10.8
0.45	14.1	16	76	17.3
0.62	10.0	22	70	23.8
0.79	8.0	28	64	30.4
0.92	6.6	34	58	35.4
1.13	5.6	40	52	43.5
1.30	4.9	46	46	50.0

Table 2. Parameters of Motor Drive System.

Parameters	Value	Unit
DC-Link Voltage	200	V
Slot/Pole Number	12/10	-
Switching Frequency	10	kHz
* Phase Resistance (R_1 + R_2)	0.5	Ω
* Phase Inductance (L_1 + L_2)	2.6	mH
* No-load Flux (λ_{m1} + λ_{m2})	0.0342	Vs
Operating Torque	1–4	Nm
Operating Speed	1200–2100	rpm

* These three parameters are tapped and change with respect to the % portion of the filter branch windings as reported in Table 1.

The values of filter capacitance, with respect to varied filter branch inductance, are calculated by specifying the f_{cut} and fmax of 2 kHz and 1.2 kHz respectively, by using (6) to (8). The value of damping resistor is chosen as 2Ω which is 1/8 times of the filter capacitive impedance (X_{CF}) at cut-off frequency. The motor was simulated through commercially used FE software "MagNet by Infolytica" where the motor speed is 2.1 kRPM and the load torque varied from 1 Nm to 4 Nm. The PWM switching currents, obtained from MATLAB/Simulink model [9], were injected into the FE model of the motor with IFI and the motor with TFI.

5.1. Impact of Filter Branch Inductance on the Motor Losses

Figure 5 shows the power losses (fundamental + PWM) of integrated motor in per-unit, with respect to filter branch inductance, at 3 Nm load torque and 2.1 kRPM rotor speed.

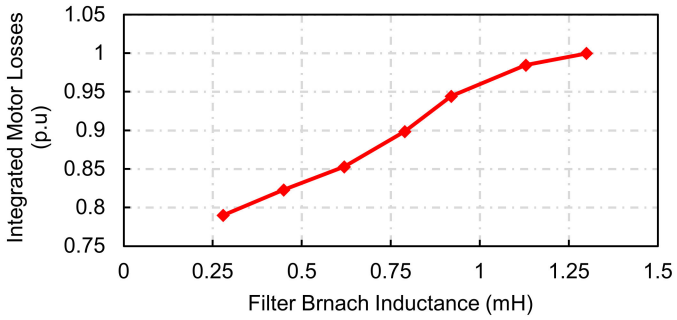

Figure 5. Power Losses of the Motor with IFI.

The per-unit values with respect to filter branch inductance were determined by dividing the loss value at 1.3 mH. It is essential to note that the I^2R power losses are ignored as they will remain unchanged due to the very small phase-shift between filter and motor branch currents [9]. As can be seen from Figure 5, the motor losses have been reduced by approximately 22% (at the lowest inductance point with respect to 1.3 mH, which is considered as a benchmark) as the inductance of the filter branch is decreased. Since the fundamental current is constant with respect to the inductance and hence the fundamental losses, the only loss affecting is the loss due to switching frequency ripple current. As we reduced the proportion of the filter branch windings, the ripple component seen by the filter branch at converter terminals will increase, however, at the same time, the motor branch windings will face more filtered and sinusoidal three-phase currents. In addition, the transformer's action has been investigated in motor branch windings when the portion of the filter branch inductance is less than the 50% of the main motor windings. In this case, both filter and motor branch windings are wound on the same slots i.e., the motor branch windings carrying switching component, which is 180° out of phase with respect to ripple component of the filter branch, as illustrated in Figure 6a,b.

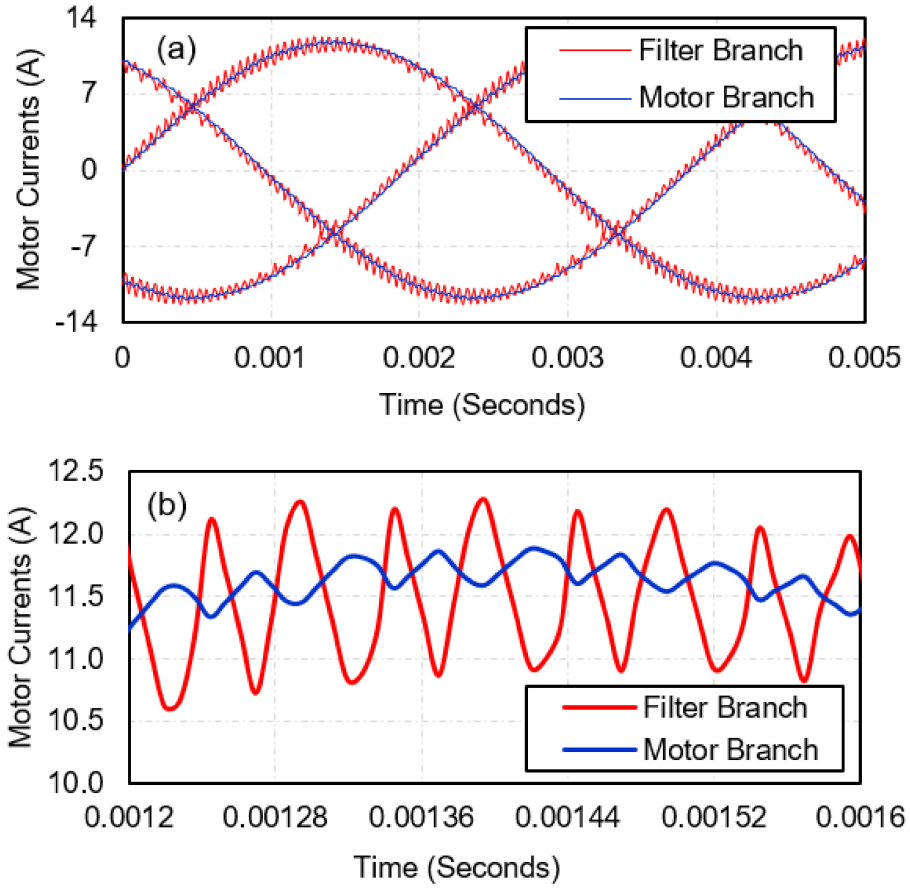

Figure 6. Transformer's Action (**a**) Filter and Motor Branch Currents (**b**) Zoom View.

5.2. Comparative Study—Traditional and Integrated Motor Drive Systems

The comparative study on the motor with TFI and the motor with IFI is carried out in terms of total system power loss, weight and volume and torque ripple on the motor shaft by using "MagNet software package by Infolytica". The EE-core filter inductor, which was designed and sized using area product approach in [4,9], is used which has the synchronous inductance of 1.3 mH, stack length of 114 mm and number of turns of 20 per phase. The synchronous inductance of EE-core filter inductor is varied by adjusting its stack length in proportion, in order to achieve the required filter inductance as per Table 1.

5.2.1. Total Loss Comparison

In this section, the comparative study of total loss for the motor with TFI and the motor with IFI is presented as shown in Figure 7a,b. The total power losses of the motor with IFI include motor stator and rotor iron loss, motor windings copper loss and the eddy current loss in the permanent magnets, whereas the total losses of the motor with TFI include motor stator and rotor iron loss, motor windings copper loss, magnet eddy current loss, inductor (i.e., EE-core) core iron loss inductor winding copper loss. The losses in the RC branch are neglected in this study as they remain unchanged for both integrated and traditional motor drive systems. From Figure 7, it can be observed that the total losses in the motor with IFI are far lower than the motor with TFI. The major loss component in the EE-core filter inductor is the iron loss which uses "M250-35A Non-oriented Mild Steel" laminations. The iron loss has considerably reduced for a motor with IFI that shares the same magnetic material (i.e., Cobalt Iron) with the motor, which was selected during the motor design phase [18,19]. Another key observation is that the total losses increase as the filter branch inductance is decreased. This is because the lower inductance of EE-core filter inductor results in an increase in switching current (seen by the inverter terminals)

yielding to higher, frequency dependent, inductor losses. On the other hand, losses in the motor with IFI have been reduced due to the fact that the switching component in the motor branch windings is compensated by the transformer's action (cf. Figure 6b).

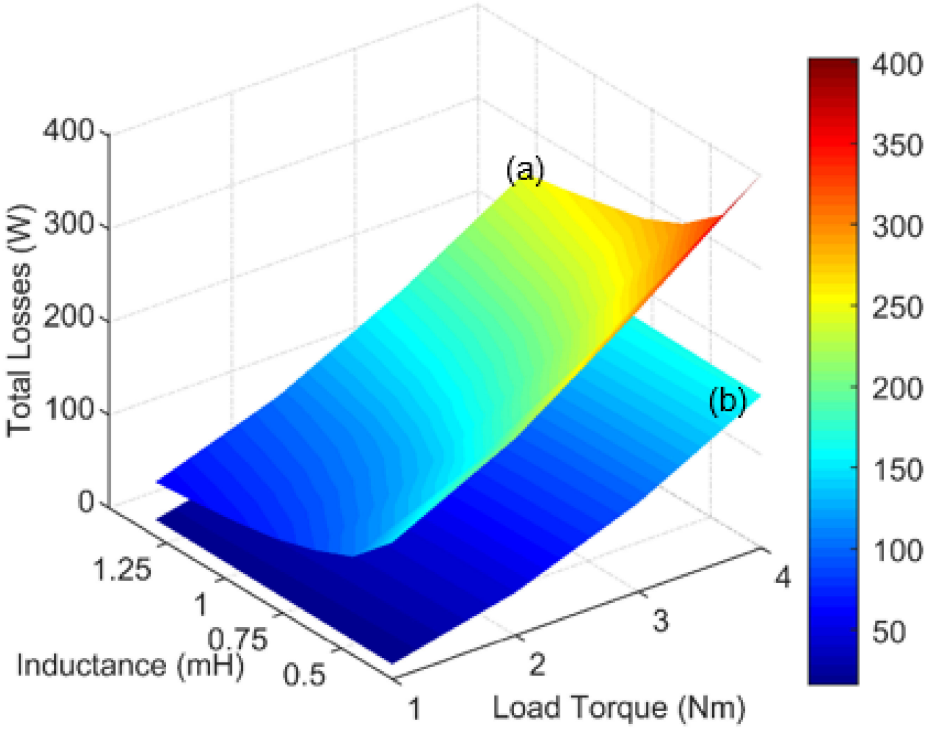

Figure 7. Total Losses with respect to Filter Branch Inductance and Load Torque (**a**) Motor with TFI (**b**) Motor with IFI.

5.2.2. Torque Ripple Comparison

Percentage torque ripple of the motor with TFI and the motor IFI have been compared, when the load torque and filter branch inductance were varied from 1 Nm to 4 Nm and 0.28 mH to 1.3 mH respectively, as shown in Figure 8. It can be observed that the torque ripple is considerably improved in the motor with IFI when the portion of filter branch is reduced from 50% (see Table 1). This is due to the switching ripple cancellation effect between the filter branch currents and the motor branch currents. In addition, the motor branch experiences more filtered currents and voltages when the portion of filter branch inductance is reduced from 1.3 mH. Therefore, decision of selecting the portion of filter branch inductance must be made upon the requirement of the torque ripple permitted by the application, since, reducing the percentage of filter branch windings will reduce the torque ripple and, at the same time, the motor branch will see the higher portion of the filtered currents and voltages but the system's weight and volume is likely to increase due to the increase in filter capacitance for the same cut-off frequency and attenuation level.

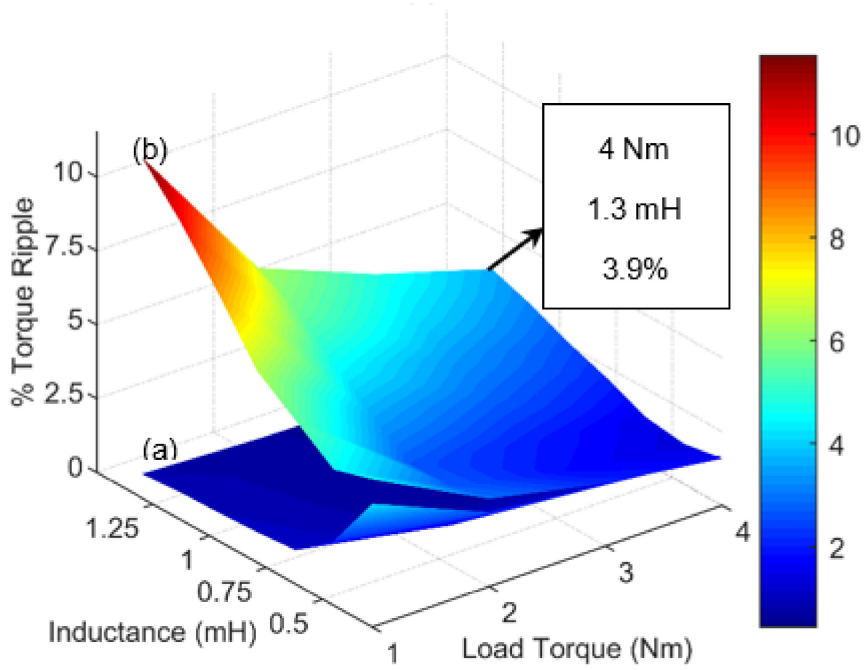

Figure 8. Percentage Torque Ripple with respect to Filter Branch Inductance and Load Torque (**a**) Motor with TFI (**b**) Motor with IFI.

5.2.3. Weight and Volume Comparison

Total system weight and volume of the motor with IFI and motor with TFI are compared as shown in Figure 9. It includes weight and volume of the motor, filter inductor, filter capacitor and damping resistor, where the capacitor's weight and volume is estimated using the datasheets of KEMET film capacitors [23]. Since the reduction in filter branch inductance increases the weight and volume of the filter capacitor therefore, from application requirement point of view, it is necessary to select the filter's parameters at which both weight and volume are minimum. The total system weight can be obtained from (15) to (16).

$$W_t = W_{core,m} + W_{core,i} + W_{cu,m} + W_{cu,i} \tag{15}$$

$$W_{core} = \rho_{core} \times V_{core} \tag{16}$$

$$W_{cu} = \rho_{cu} \times V_{cu} = \rho_{cu} \frac{\pi}{4} D^2 MLT \times m \times N_{ph} \tag{17}$$

where, $W_{core,m}$ and $W_{core,i}$ are the weight of the motor and inductor iron core in kg respectively, $W_{cu,m}$ and $W_{cu,i}$ are the weight of the motor and inductor copper windings in kg respectively, ρ_{core} and ρ_{cu} are the mass density of ferrous and copper material in kg/m^3 respectively, D is the bare copper diameter of wire used in motor or inductor, MLT is the mean length per turn, m is the number phases, N_{ph} is the number of turns per phase and V_{core} is the volume of the ferrous core used in motor or inductor. In this study, weight of the ferrous core is determined via finite element by integrating the mass density of core component, therefore, by using (16), the volume of the motor or inductor ferrous core can be obtained. The total system volume is obtained using (18) to (20),

$$V_t = V_{mot} + V_{ind} \tag{18}$$

$$V_t = \frac{\pi}{4} D_{out}^2 \times L_m \tag{19}$$

$$V_i = \mathrm{A} \times B \times L_i \tag{20}$$

where V_t is the total system volume in kg, V_{mot} is the total motor volume in kg, V_{ind} is the total volume of the external inductor, D_{out} is the outer diameter of the motor including

housing, L_m is the full length of the machine including end-windings overhung and housing endcaps, A and B are height and width of the inductor and L_i is the full length of the inductor including end-windings overhung. It is important to note that the volume of the inductor (V_{ind}) is zero, in the case of motor with integrated filter inductor.

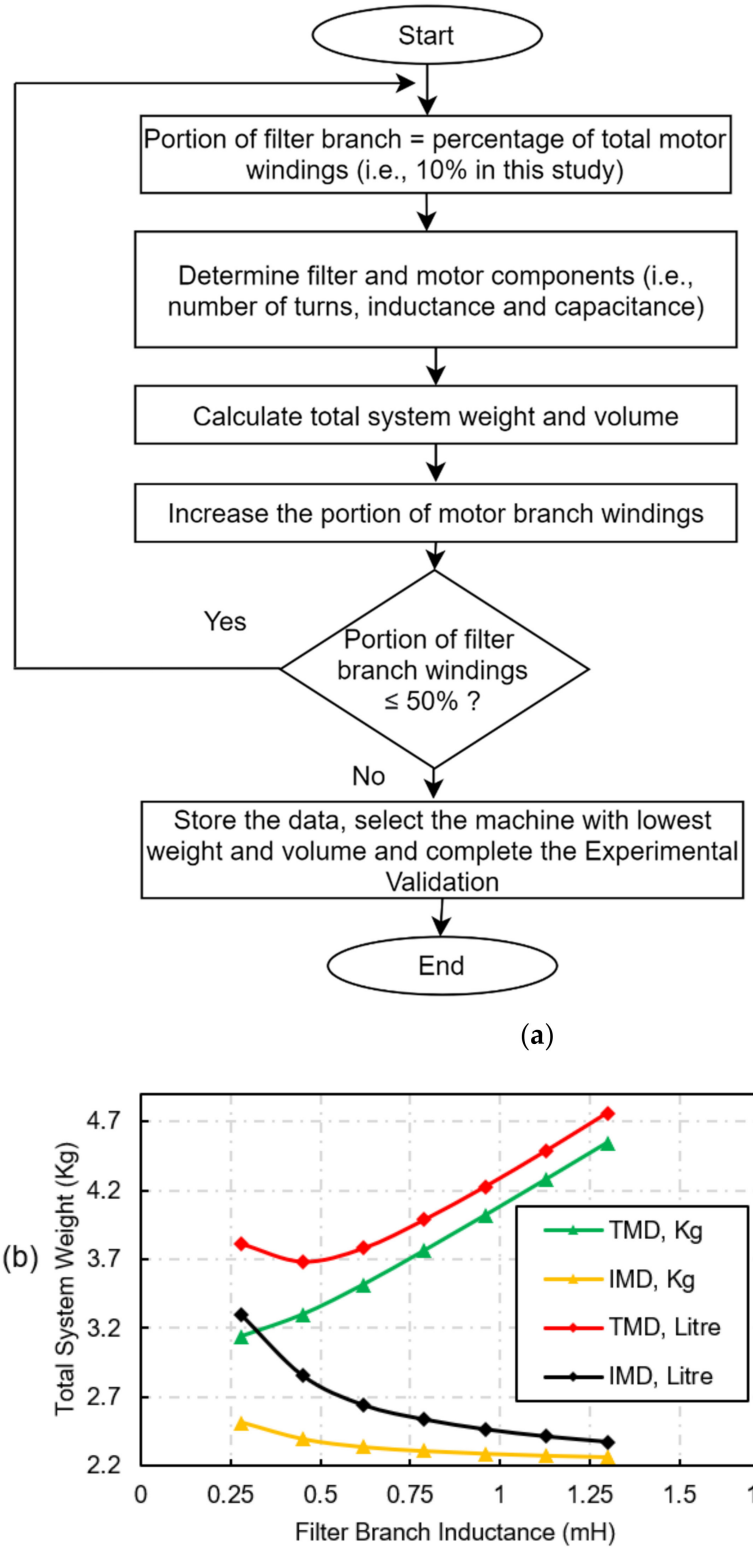

Figure 9. (**a**) Flow chart of the optimization work (**b**) Weight and Volume Comparison, where TMD refers to Traditional Motor Drive System and IMD refers to Integrated Motor Drive System.

Figure 9a shows the flow chart of the optimization work that has been carried out to minimize the total system mass and volume of the motor drive. It should be noted here that the % portion of the filter branch is not varied beyond 50% due to the fact that the filtering effect on the motor winding will start to reduce as the motor will experience more PWM voltages on higher portion of its windings.

As can be seen from Figure 9, the volume of the motor with TFI reduces as the filter inductance is decreased until 0.45 mH and then, begins to rise until 0.28 mH. This is because the volume of the inductor dominates the volume of the capacitor before and after 0.45 mH. At this point (i.e., 0.45 mH), the inductor's volume is 1/3rd of the volume at 1.3 mH and the capacitor's volume is 2.9 times the weight at 1.3 mH. In terms of mass, the overall system's weight reduces as the filter inductance is reduced for the motor with TFI since the inductor's weight throughout dominates i.e., increase in capacitance does not affect the overall system's weight. On the other hand, the inductor's volume is zero in the motor with IFI, therefore, its overall volume increases as the filter branch winding inductance is reduced (or the filter capacitance is increased). However, the weight of the motor with IFI follows the same trend as in the case of volume i.e., total weight increases as the filter branch winding inductance is reduced due to the absence of inductor's volume. As expected, the total system's weight and volume have increased (but it is still significantly lesser than the motor with TFI) as the filter branch inductance is reduced due to the capacitor's weight added with the motor.

The optimal point, where system's weight and volume are minimum, is 1.3 mH i.e., 50% filter branch portion compared to the entire motor winding. Considering the allowable torque ripple of $\pm$10% at the rated load conditions, the magnitude of the torque ripple (i.e., 3.9%) is less than the accepted value given by the application (cf. Figure 8), which does not pose any risk to the mechanical load acting on the shaft. Therefore, 50% portion of filter branch winding is finalizedan and selected for the concept validation of the motor with IFI, aiming to minimize the total system weight and volume.

6. Experimental Study and Validation

In this section, the experimental study is conducted in order to validate the motor with IFI, presented in Section 3, with 50% portion of the filter branch windings. This machine was built for the HEMAS project, in the recent years, at The University of Nottingham [18,19].

6.1. Test Setup

The test setup for the concept validation of the motor with IFI, when the filter branch inductance is 1.3 mH, is shown in Figures 10 and 11. The Spectra Quest's Drivetrain Diagnostics Simulator (Figure 10) is used which is specifically designed to simulate industrial drivetrains for experimentation of the motors under test. The drivetrain consists of an electric motor under test, torque transducer, gearbox system, bearing loader, speed encoder and magnetic brake [24]. In order to drive the motor under test, 3-phase, voltage source converter, which was particularly designed for HEMAS project, is used. It consists of a three-phase IGBT module, sensors and the gate-drive circuit which are integrated with a shared control system based on FPGA, DSP and DC-link LC filter. The DSP unit communicates with the swashplate control computer (SPCC) for control and monitoring purposes and estimates the modulation index for the PWM pulse, whereas, FPGA is used to interface with the sensor circuit and for the PWM pulse generation [19]. The prototype of 12 slots/10 poles, concentrated wound machine, is depicted in Figure 12a,b, where windings A_2, B_2 C_2 represent motor branch and A_1, B_1 C_1 correspond to the filter branch (i.e., when the filter branch portion is 50%). The RC branch of the filter circuit consist of three wire wound damping resistors (5 W and 2 Ω), and three KEMET film type capacitors (4.7 μF each, Model no. R46KR447050M2K) [20] as shown in Figure 12c.

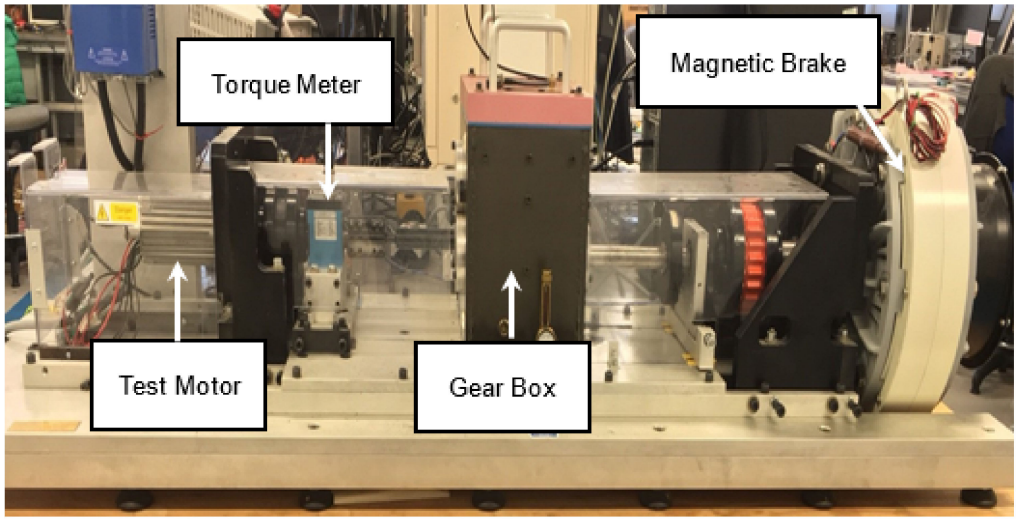

Figure 10. Experimental Setup—Spectra-Quest's Rig.

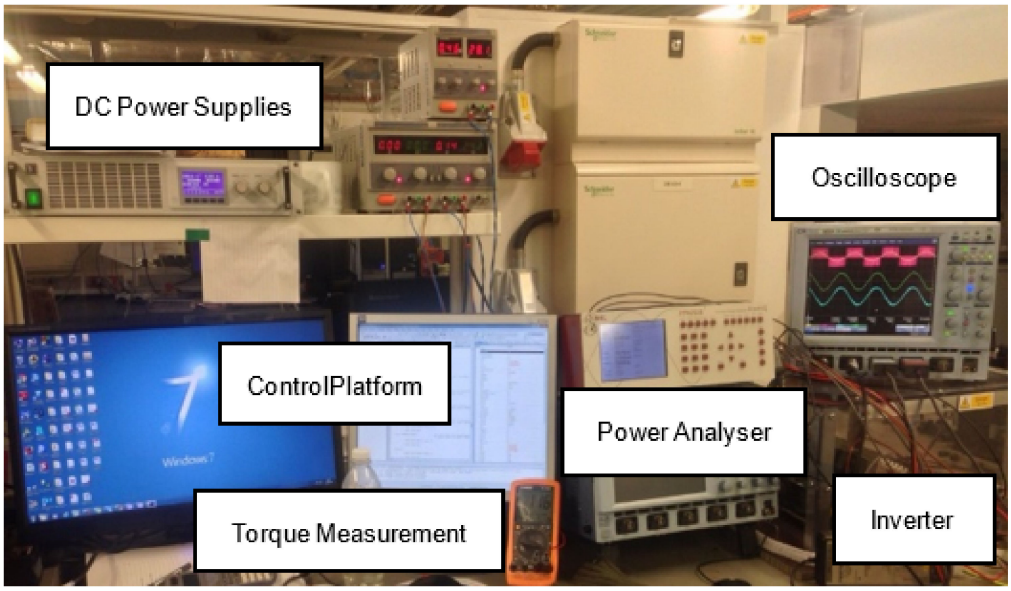

Figure 11. Control Platform of Testing Motor with IFI.

6.2. Results and Discussion

The experimental results of the motor with IFI are shown in Figure 13, when the rotor is rotating at 2.1 kRPM and load torque of 4 Nm is applied using magnetic bake. Figure 13a shows the inverter/converter side voltage and the motor branch voltage, where their corresponding FFTs are shown in Figure 13b. Figure 13c shows the filter and motor branch currents, whilst, the output torque, at the rated condition, is depicted in Figure 13d. From Figure 13b, it can be observed that the motor with IFI is able to remove unwanted switching component of the inverter from the motor terminals, thus, eliminating the high frequency power losses and the high frequency voltage stress from the motor. The magnitude of the motor voltage at 20 kHz is reduced from 62.3 V to 1.3 V, which is a reduction of 97.9% reduction. It can be argued that the filter branch windings still experience PWM voltages and currents. Therefore, insulation system of filter branch windings must be enhanced to protect it from over-voltages and the high dv/dt. This is, in particular, a problem when long feeder cables are used between converter and the motor terminals which is not the case for the application under consideration. Figure 13d shows the torque ripple of the motor at rated load. Due to low precision of DDS's torque meter the measured torque was estimated

using (20), where the instantaneous values of measured back-EMF (e_{1abc}, e_{1abc}) and measured currents (Figure 13c) were used.

$$T_{out} = K_t\left(\frac{e_{1a}i_{1a}}{\omega_e} + \frac{e_{1b}i_{1b}}{\omega_e} + \frac{e_{1c}i_{1c}}{\omega_e}\right) + K_t\left(\frac{e_{2a}i_{2a}}{\omega_e} + \frac{e_{2b}i_{2b}}{\omega_e} + \frac{e_{2c}i_{2c}}{\omega_e}\right) \quad (21)$$

The no-load voltage was measured at the motor terminals by decoupling the motor shaft from the load. The FFT of the no-load voltage confirms that the motor is free from the low order harmonics, therefore, back-EMF in (15) can be consider sinusoidal in order to estimate the output torque and torque ripple by using measured 3-phase currents. The torque ripple, as shown in Figure 13d, is computed as 6.2%, where the 20 kHz switching component is shown. This is an order of magnitude less than the allowable torque ripple from the application. The torque ripple, in this motor, is mainly caused by the harmonics presented in the current waveform since the HEMAS motor was designed to have a sinusoidal back-EMF and the minimum cogging torque (in the order of 0.004 Nm), as confirmed by FEA in Figure 14. The magnitude of percentage current ripple is plotted, as shown in Figure 15, with respect to the rotor speed and the load torque. The rotor speed is adjusted from 1.2 kRPM to 2.1 kRPM, whereas load torque is varied from 1.5 Nm to 4 Nm. The % current ripple of filter branch winding currents and the motor branch windings currents are reduced as the load torque on the motor shaft is increased. This is because the inverter's switching ripple is mainly dependent on the inductance of the filter circuit which usually remains constant w.r.t mechanical load, provided operating under saturation. The in-depth comparative study of the motor without RLC output filter, motor with IFI and the motor with TFI is presented in [9].

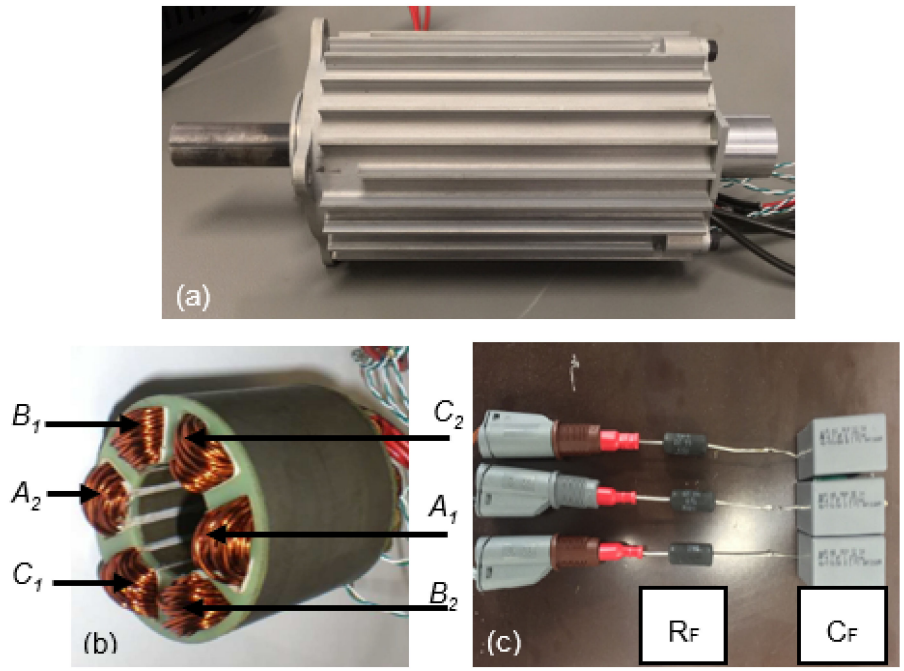

Figure 12. Integrated Motor Prototype with Arrangement of the windings (**a**) Motor with Casing (**b**) Motor without Casing (**c**) 3-phase Damping Resistors and 3-phase Filter Capacitors connected in star connection.

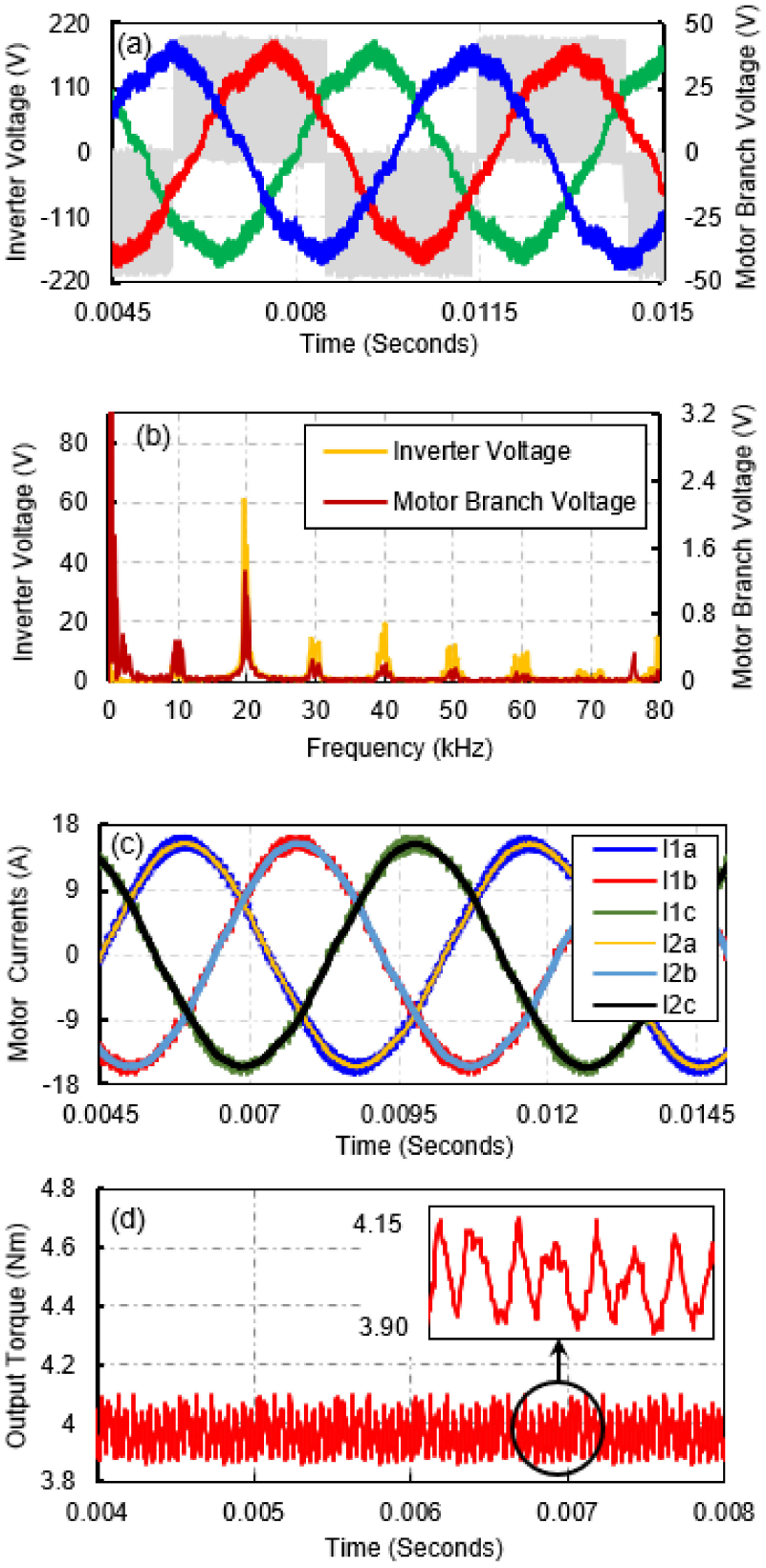

Figure 13. Experimental Results (**a**) Inverter and Motor Branch Voltages (**b**) FFT of Inverter Voltage and Motor Branch Voltage (**c**) Filter and Motor Branch Currents (**d**) Torque at 4 Nm and 2.1 kRPM with 20 kHz switching component.

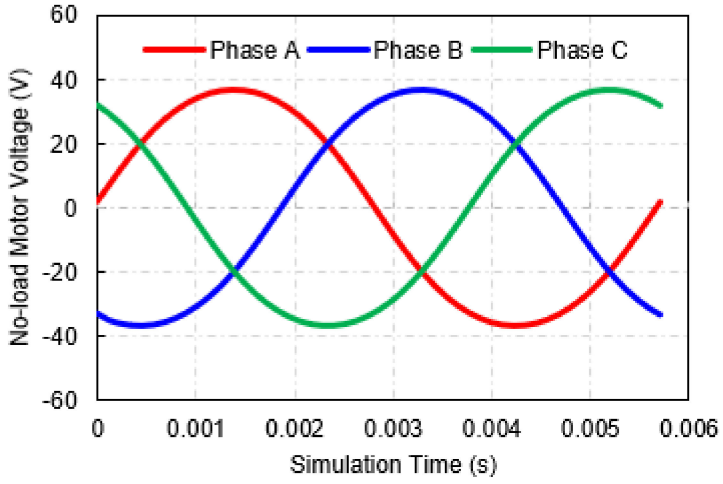

Figure 14. Back-EMF of the Integrated Motor based on FE Model.

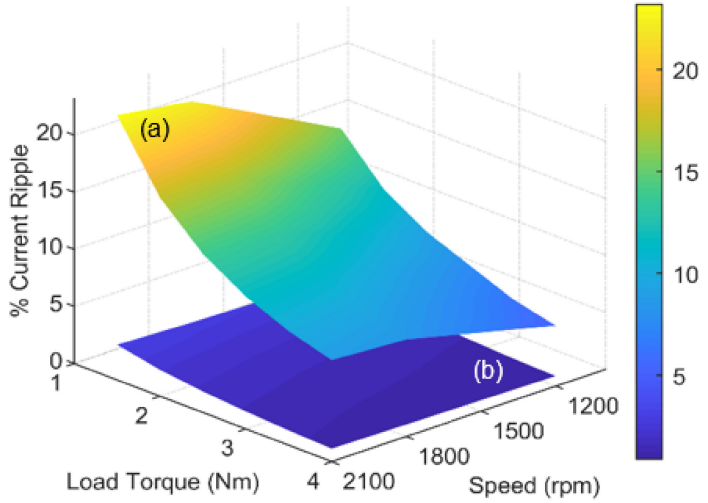

Figure 15. Percent Current Ripple vs. Speed and Torque (**a**) Filter Branch Current Ripple (**b**) Motor Branch Current Ripple.

7. Conclusions

The performance optimization of the integrated motor drive system has been presented in this paper where the IFI is used for an aerospace actuator motor, which forms a part of RLC output filter. The motor with IFI entirely eliminates the need for a traditional EE-core filter inductor by using the inherent motor's magnetics. This removes the associated losses, weight and volume from the system. The optimization of filter branch windings was done, where the filter branch was tapped, aiming to reduce the mass and volume and to improve performance parameters such as power loss and torque ripple. The study has shown that the high frequency ripple cancellation effect has been taken place when the portion of filter branch is less than 50% of the entire motor windings which improves the power losses and torque ripple performance, caused by the high frequencies. However, the optimum weight and volume were found when the portion of filter branch windings is 50%.

The experimental validation of the motor with IFI showed that the proposed integration concept is feasible and can be practically implemented which comes with an advantage of not having the standard discrete inductor in the motor-drive system. Thus, the penalty of added inductor losses, weight, volume and its associated manufacturing cost is eliminated completely. Although the proposed approach offers these benefits, it comes with the drawback of needing a better insulation system for the filter branch since the PWM

voltage constantly stresses the motor windings which may not be an ideal case scenario for applications where converter is operated with very high switching frequency (can go up to 50 to 100 kHz) and very low rise-time (in the range of 1 to 5 nanoseconds). Therefore, when implementing the proposed approach, special care must be taken whilst selecting the wire insulation (i.e., insulation thickness or material type such as organic, inorganic or both) of the filter branch windings.

Author Contributions: Conceptualization, M.R.K., C.G. and G.V.; methodology, M.R.K. and G.V.; software, M.R.K.; validation, M.R.K., C.P. and S.O.; formal analysis, M.R.K.; investigation, M.R.K.; resources, M.R.K.; data curation, M.R.K.; writing—original draft preparation, M.R.K.; writing—review and editing, M.R.K., G.V. and S.O.; visualization, G.V. and S.O.; supervision, C.G., G.V. and C.P.; project admin-istration, C.G. and G.V.; funding acquisition, C.G., P.W. and G.V. All authors have read and agreed to the published version of the manuscript.

Funding: This research received no external funding.

Institutional Review Board Statement: Not Applicable.

Informed Consent Statement: Not Applicable.

Data Availability Statement: Not Applicable.

Conflicts of Interest: The authors declare no conflict of interest.

References

1. Sarlioglu, B.; Morris, C.T. More Electric Aircraft: Review, Challenges, and Opportunities for Commercial Transport Aircraft. *IEEE Trans. Transp. Electrif.* **2015**, *1*, 54–64. [CrossRef]
2. Madonna, V.; Giangrande, P.; Galea, M. Electrical Power Generation in Aircraft: Review, Challenges, and Opportunities. *IEEE Trans. Transp. Electrif.* **2018**, *4*, 646–659. [CrossRef]
3. Bozhko, S. Towards Smart Electric Power Systems in Future Aircrafts. Available online: http://ieps.kpi.ua/wp-content/uploads/2016/08/Bozhko.pdf (accessed on 22 July 2020).
4. Khowja, M.R.; Gerada, C.; Vakil, G.; Abebe, R.; Odhano, S.; Patel, C.; Wheeler, P. Novel Motor-Shaped Rotational Inductor for Motor Drive Applications. *IEEE Trans. Ind. Electron.* **2019**, *67*, 1844–1854. [CrossRef]
5. Kimura, S.; Itoh, Y.; Martinez, W.; Yamamoto, M.; Imaoka, J. Downsizing effects of integrated magnetic components in high power density DC–DC converters for EV and HEV applications. *IEEE Trans. Ind. Appl.* **2016**, *52*, 3294–3305. [CrossRef]
6. Walker, A.; Vakil, G.; Gerada, C. Novel core designs to miniaturise passive magnetic components. In Proceedings of the 2018 IEEE Transportation Electrification Conference and Expo (ITEC), Long Beach, CA, USA, 13–15 June 2018; pp. 644–649.
7. Abebe, R.; Vakil, G.; Lo Calzo, G.; Cox, T.; Lambert, S.; Johnson, M.; Gerada, C.; Mecrow, B. Integrated motor drives: State of the art and future trends. *IET Electr. Power Appl.* **2016**, *10*, 757–771. [CrossRef]
8. Popovic, J.; Ferreira, J.A.; Gerber, M.B.; Konig, A.; Doncker, R.D. Integration technologies for high power density power electronic converters for AC drives. In Proceedings of the International Symposium on Power Electronics, Electrical Drives, Automation and Motion, Taormina, Italy, 23–26 May 2006; pp. 634–639.
9. Khowja, M.R.; Gerada, C.; Vakil, G.; Patel, C.; Odhano, S.; Walker, A.; Wheeler, P. Novel Permanent Magnet Synchronous Motor with Integrated Filter Inductor, Using Motor's Inherent Magnetics. *IEEE Trans. Ind. Electron.* **2021**, *68*, 5638–5649. [CrossRef]
10. Khowja, M.R.; Gerada, C.; Vakil, G.; Wheeler, P.; Patel, C. Integrated Output Filter Inductor for Permanent Magnet Motor Drives. In Proceedings of the Industrial Electronics Society, IECON 2016-42nd Annual Conference of the IEEE, Florence, Italy, 23–26 October 2016.
11. Khowja, M.R.; Gerada, C.; Vakil, G.; Wheeler, P.; Patel, C. Novel integrative options for passive filter inductor in high speed AC drives. In Proceedings of the IECON 2016-42nd Annual Conference of the IEEE Industrial Electronics Society, Florence, Italy, 23–26 October 2016; pp. 1137–1142.
12. La Rocca, A.; Khowja, M.R.; Vakil, G.; Gerada, C.; Wheeler, P.; Yan, L. Thermal Design of an Integrated Inductor for 45kW Aerospace Starter-Generator. In Proceedings of the 2020 IEEE Transportation Electrification Conference & Expo. (ITEC), Chicago, IL, USA, 23–26 June 2020; pp. 703–708.
13. Garvey, S.D.; Norris, W.T.; Wright, M.T. The role of integrated passive components in protecting motor windings. *IEE Proc. Electr. Power Appl.* **2000**, *147*, 367–370. [CrossRef]
14. Deng, X.; Mohamed, M.A.S.; Lambert, S.; Mecrow, B. Development of a High-Speed, Permanent Magnet, SiC-Based Drive with Integrated Input Filters. *IEEE Trans. Energy Convers.* **2020**, *35*, 863–874. [CrossRef]
15. Deng, X.; Lambert, S.; Mecrow, B.; Mohamed, M.A.S. Design Consideration of a High-Speed Integrated Permanent Magnet Machine and its Drive System. In Proceedings of the 2018 XIII International Conference on Electrical Machines (ICEM), Alexandroupoli, Greece, 3–6 September 2018; pp. 1465–1470.

16. Stratta, A.; Mouawad, B.; Ahmadi, B.; Lillo, L.d.; Empringham, L.; Johnson, M. A novel manufacturing technique for integrating magnetic components windings on power module substrates. In Proceedings of the 2019 21st European Conference on Power Electronics and Applications (EPE '19 ECCE Europe), Genova, Italy, 3–5 September 2019; pp. 1–8.
17. Saeed, R.; Johnson, C.M.; Empringham, L.; Lillo, L.D. High current density air cored Inductors for direct power module integration. In Proceedings of the 2014 16th European Conference on Power Electronics and Applications, Lappeenranta, Finland, 26–28 August 2014; pp. 1–6.
18. Rottach, M.; Gerada, C.; Wheeler, P. Evaluation of motor-drive segmentation strategies for fault-tolerance. In Proceedings of the 2013 IEEE ECCE Asia Downunder, Melbourne, Australia, 3–6 June 2013; pp. 530–536.
19. Rottach, M.; Gerada, C.; Wheeler, P. Design optimisation of a fault-tolerant PM motor drive for an aerospace actuation application. In Proceedings of the 7th IET International Conference on Power Electronics, Machines and Drives (PEMD 2014), Manchester, UK, 8–10 April 2014.
20. Khowja, M.R.; Vakil, G.; Gerada, C. Analytical Tool to Generate Torque-Speed Characteristics for Surface Mounted PM Machines in Constant Torque and Field Weakening Regions. In Proceedings of the IECON 2019-45th Annual Conference of the IEEE Industrial Electronics Society, Lisbon, Portugal, 14–17 October 2019; pp. 922–927.
21. Hanigovszki, N.; Landkildehus, J.; Blaabjerg, F. Output filters for AC adjustable speed drives. In Proceedings of the APEC 07-Twenty-Second Annual IEEE Applied Power Electronics Conference and Exposition, Anaheim, CA, USA, 25 February–1 March 2007; pp. 236–242.
22. Sozer, Y.; Torrey, D.A.; Reva, S. New inverter output filter topology for PWM motor drives. IEEE Trans. *Power Electron.* **2000**, *15*, 1007–1017. [CrossRef]
23. Huber, L.; Borojevi, D. Space vector modulated three-phase to three-phase matrix converter with input power factor correction. *IEEE Trans. Ind. Appl.* **1995**, *31*, 1234–1246. [CrossRef]
24. She, H.; Lin, H.; Wang, X.; Yue, L. Damped input filter design of matrix converter. In Proceedings of the 2009 International Conference on Power Electronics and Drive Systems (PEDS), Taipei, Taiwan, 2–5 November 2009; pp. 672–677.